

ReSKETCH: A Mergeable, Partitionable, and Resizable Sketch

Vinh Quang Ngo
Chalmers University of Technology
and Gothenburg University
Gothenburg, Sweden
vinhq@chalmers.se

Martin Hilgendorf
Chalmers University of Technology
and Gothenburg University
Gothenburg, Sweden
martin.hilgendorf@chalmers.se

Marina Papatriantafilou
Chalmers University of Technology
and Gothenburg University
Gothenburg, Sweden
ptrianta@chalmers.se

ABSTRACT

1 Tracking items' frequency in data streams is a fundamental problem
2 with applications ranging from network monitoring to database
3 query optimization, machine learning, and more. Sketches offer
4 practical, sublinear-memory solutions that provide high-throughput
5 updates and queries with provable accuracy approximation bounds.
6 Furthermore, sketches are mergeable, which allows multiple ones
7 of identical parameters to be combined into a single, representative
8 sketch, which enables their use in parallel and distributed systems.

9 Still, there are limitations in known sketch designs that restrict
10 their applicability in systems characterized by resource heterogeneity
11 across nodes, workload fluctuation over time, and the need for
12 efficient distributed data aggregation. We identify and formalize
13 three critical properties that can address these limitations: *resizability*,
14 *enhanced mergeability*, and *partitionability*. We propose ReSKETCH,
15 a matrix-based sketch algorithmic design, which, through a
16 combination of consistent hashing and quantile sketching, fused
17 with a partition-aware hashing technique, leads to the ability to
18 satisfy all three properties, with a beneficial memory-to-accuracy
19 ratio. We propose an analysis methodology for dynamic sketches
20 and apply it to investigate the costs and benefits of ReSKETCH,
21 in conjunction with a detailed empirical study that also includes
22 its time-associated behavior. As ReSKETCH is orthogonal to other
23 matrix-based sketches, we expect it can enable them to support the
24 aforementioned properties and, in turn, lead to new significant use
25 cases for frequency estimation sketches in modern systems.

PVLDB Reference Format:

Vinh Quang Ngo, Martin Hilgendorf, and Marina Papatriantafilou.
ReSKETCH: A Mergeable, Partitionable, and Resizable Sketch. PVLDB, 18(9):
XXX-XXX, 2025.
doi:XX.XX/XXX.XX

PVLDB Artifact Availability:

The source code, data, and/or other artifacts have been made available at
<https://github.com/vinhqngo5/ReSketch>.

1 INTRODUCTION

Tracking item frequencies and derivative problems such as heavy hitter detection [7, 10, 27, 35], estimation of frequency moments [18], inner products [3], and range sums [15] are fundamental primitives

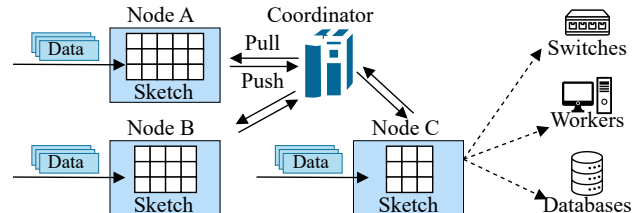


Figure 1: Distributed monitoring with heterogeneous nodes and dynamic workload maintaining sketches of varying sizes.

for data-intensive systems. They are used for query optimization, approximate query processing, and join size estimation in databases [1, 28, 29]; identifying popular flows, DDoS mitigation, and change detection in networking [9, 17, 36]; load balancing and caching in distributed systems [30]; and more. Given the input rate of such systems, it is important to find algorithms that have favorable memory requirements and capabilities to process streams promptly in a single pass. Knowing that the exact solutions require memory at least linear to the number of distinct items in the data [14], and that many applications accept some approximation, a substantial volume of work focuses on succinct (sublinear) representations from which items' frequencies can be queried approximately.

A common approach achieving this is through frequency estimation sketches [7, 11], which provide (ϵ, δ) -approximation; i.e. item frequencies are estimated with a bounded approximation factor ϵ , with probability at least $1 - \delta$. They are commonly implemented as $w \times d$ -matrices (width \times depth), in which w influences ϵ , while d influences the probability bound δ . A valuable property of sketches is mergeability [2], meaning that multiple sketches of size $w \times d$ can be combined into one with the same size and (ϵ, δ) guarantee. This property makes sketches even more powerful, providing better scalability and flexibility, which enables broader use-cases such as distributed data processing and in-network aggregation [2]. However, as systems turn more *distributed*, *heterogeneous*, and *dynamic*, there is an increasing need for solutions that go beyond what conventional sketch designs and their mergeability can address.

The need for more flexible sketches. Let's consider an example distributed network monitoring system as illustrated in Figure 1, where network devices monitor traffic flows using sketches. Note that (i) Due to *heterogeneity* in device capabilities and *dynamicity* in resources and traffic, both the available memory and the needed space for sketching vary both across devices and over time, which creates the need for adaptive memory allocation. (ii) For query processing, devices periodically send their sketches to a coordinator, which merges them (if possible) before querying or otherwise scans all of them; when sketch sizes are heterogeneous, there is no known method to merge them, and all sketches must be scanned. (iii) As

This work is licensed under the Creative Commons BY-NC-ND 4.0 International License. Visit <https://creativecommons.org/licenses/by-nc-nd/4.0/> to view a copy of this license. For any use beyond those covered by this license, obtain permission by emailing info@vldb.org. Copyright is held by the owner/author(s). Publication rights licensed to the VLDB Endowment.

Proceedings of the VLDB Endowment, Vol. 18, No. 9 ISSN 2150-8097.
doi:XX.XX/XXX.XX

Table 1: Analysis and state-of-the-art of sketch properties in focus: motivation, related work, and gaps.

Property	Motivation	Related Work	Gap
Resizability	Error bounds (ϵ, δ) are fixed at initialization, based on dimensions $w \times d$ and cannot be changed without initializing new sketches. <i>Expandability</i> can improve accuracy when resources become available; <i>shrinkability</i> can free memory for other tasks or reduce transmission overhead.	Some methods support expandability [38], others shrinkability [36], mostly at coarse granularity (doubling or halving the size) rather than fine-grained adjustments. Only Geometric Sketch (GS) [4] supports fine-grained expansion and memory release.	GS cannot shrink below its initial allocation, and its throughput reduces as it expands. If initialized too small (which allows it to shrink to a smaller size when needed), frequent expansion reduces throughput and degrades accuracy.
Enhanced Mergeability	<ul style="list-style-type: none"> Conventional mergeability requires identical dimensions (cannot merge differently-sized sketches). Cannot control the output size when merging to control precision. E.g., when p devices maintain sketches of size $w \times d$, they consume $p \times w \times d$ space but can only achieve single-sketch accuracy after merging. 	Resizing the sketches before merging (<i>resize-then-merge</i>) seems like a straightforward solution. However, existing resizable sketches GS and DCMS [4, 38] still logically stack multiple fixed-size sketches internally, so resizing does not make them compatible for merging.	<ul style="list-style-type: none"> No support for merging heterogeneous-sized sketches, which implies scanning all sketches during queries, plus bookkeeping overhead. Even when merging the same-sized sketches, cannot control the output size to preserve higher precision.
Partitionability	As workloads scale, partitioning traffic across multiple sketch instances (e.g., offloading a subset of keys and their counts to a new node) is essential for load balancing and parallel processing. Dynamic environments further require moving partitions (and their state) between nodes at runtime.	Partitioning streams to independent sketches improves throughput and accuracy [16, 18, 20, 27, 32]. Known approaches rely on <i>static partitioning</i> defined at initialization.	Cannot dynamically rebalance partitions or migrate state (historical data) between sketches.

75 devices join or leave the network due to load balancing or reconfiguration, the system must redistribute monitoring responsibilities
76 while preserving historical information.

77 These observations motivate three properties: **1 Resizability**—the ability to dynamically expand or shrink the sketch size
78 at fine granularity while maintaining accuracy and throughput
79 comparable to a sketch initialized at the target size; **2 Enhanced**
80 **Mergeability**—the ability to combine sketches of different sizes
81 and control the output size to preserve as much precision as the
82 input sketches collectively offer; **3 Partitionability**—the ability
83 to partition the sketch state itself (not just the input) to enable
84 dynamic redistribution of monitoring responsibilities while pre-
85 serving historical information. Table 1 summarizes the motivation,
86 related work, and existing gaps for each property.

87 *Insights.* The observed limitations stem from a single, funda-
88 mental design choice inherent in customary sketches: the hash
89 functions. For a sketch of size $w \times d$, existing designs employ d
90 functions h_1, \dots, h_d drawn from a pairwise independent family.
91 In the de facto standard approach, these functions determine the
92 bucket index $h_i(e)$ for an item e via a modulo operation (\pmod{w}).
93 This mapping is static and does not change over time, which is not
94 flexible enough to support the aforementioned requirements. Con-
95 sider resizing a sketch by changing its width from w to w' ; there
96 will be excessive need for moving contents of buckets to other ones,
97 and, moreover, as the counters within a bucket are aggregations of
98 counts, when a bucket's contents must be remapped due to resiz-
99 ing, merging, or partitioning, there is no information to guide the
100 process. E.g., if a counter at a single bucket needs to be partitioned
101 across two new buckets, known methods cannot determine how to
102 partition its value because we do not know *which items are present*
103 or *their individual counts* to map to the new locations.

104 *Contributions.* We identify and formalize three critical properties—
105 *resizability*, *enhanced mergeability*, and *partitionability*—that extend
106 the applicability of frequency estimation sketches, and propose

RESKETCH, a *sketch algorithmic design* that achieves all three. In
109 particular, RESKETCH builds on a novel coupling of *three key ideas*:
110

111 First, instead of using the conventional modulo-based bucket
112 mapping, we transform each bucket's responsible domain from dis-
113 crete to continuous using *consistent hashing* [21]. The hash space
114 over which bucket responsibility is defined is conceptualized as a
115 continuous logical ring (e.g., the interval $[0, 1]$). The sketch's buck-
116 etes are then defined as contiguous, non-overlapping *segments* that
117 partition the ring. An item is assigned to the single bucket whose
118 segment covers the item's hash value. The hash function *mapping*
119 *items to the ring remains fixed* for the sketch's lifetime. Structure-
120 defining operations, such as resizing or partitioning, are performed
121 not by changing the function, but by *adjusting the boundaries* that
122 define the segments. These boundaries are initialized as points cho-
123 sen uniformly at random on the ring by pairwise independent hash
124 functions, which ensures a balanced distribution across buckets.

125 Second, based on the above, redistributing items during resiz-
126 or partitioning reduces to identifying the portion of a segment (i.e.,
127 which *few items*) should be moved. Hence, we define a “sketch of
128 sketches” design that maintains a per-bucket mergeable distribution
129 summary (e.g., a quantile sketch) that approximates the distribu-
130 tion of items' hash values within that bucket. When a segment is
131 resized or moved, we query that summary to estimate the counts
132 corresponding to the portion of the segment being moved. Also,
133 since the quantile summary is mergeable, it makes the aforemen-
134 tioned *resize-then-merge* strategy possible, thereby enabling both
135 *resizability* and *enhanced mergeability*. The extra information in
136 the quantile summary also enables a new, improved estimator for
137 items' frequencies, which compensates for the extra memory used.

138 Third, to enable sketch partitioning, we introduce **Partition-
139 Aware Hashing**. In sketches, an item is scattered to random buck-
140 etes across rows. Consequently, simply partitioning the sketch by
141 column index (e.g., assigning the first half of columns to one sketch
142 and the rest to another) is ineffective: a single item's hash locations

would span both partitions, which makes future updates be sent to multiple sketches. Our approach solves this by assigning every item a *fingerprint* that maps it to exactly one partition at any given time. These partitions correspond to segments in a global partition ring (i.e., different from the per-row rings discussed), with each segment corresponding to a sketch. During a sketch partition operation, an item may be reassigned to a new partition (sketch). Its history and newer updates can find the new partition easily through the *fingerprint* and its segment in the partition ring. Importantly, we recover this fingerprint directly from the stored hash values in the aforementioned quantile sketch using *modular multiplicative inverses*, which requires no additional storage overhead.

Besides these ideas and their synthesis forming ReSKETCH, we provide a methodology to analyse properties of dynamic sketches, proposing the concept of an *instance-provenance graph*, show analytical bounds for the algorithm, present an open-source repository with an implementation [26], as well as a comprehensive experimental evaluation on both real-world and synthetic datasets. The results demonstrate that ReSKETCH achieves high accuracy and competitive throughput even with small space needs, while providing the three desired properties, outperforming state-of-the-art baselines that only partly address some of these properties.

Importantly, because the proposed mechanisms are compatible with matrix-based sketches, other sketches can adopt this design to inherit resizability, enhanced mergeability, and partitionability. Moreover, ReSKETCH complements and extends recent works including [18, 20, 27, 32], which have shown that splitting the input domain and sketching each such partition separately yields orders-of-magnitude improved accuracy/memory ratio for frequency moments and frequent items sketching, while also enabling concurrency. ReSKETCH provides significant steps towards addressing the questions of how partitions of keys to such sketches can happen in general and with what dynamic properties. We expect ReSKETCH’s approach to unlock significant new possibilities for frequency estimation sketches in modern, dynamic systems.

Roadmap. The rest of the paper is organized as follows. § 2 provides preliminaries on frequency estimation sketches and their mergeability. § 3 formalizes the three properties. § 4 presents the design of ReSKETCH. § 5 provides theoretical analysis. § 6 presents experimental results. Finally, § 7 concludes the paper.

2 PRELIMINARIES

Count-Min Sketch. Count-Min Sketch (CMS) [11] is a probabilistic data structure that provides approximate frequency counts of items in a data stream. Let $S = \langle e_1, e_2, \dots \rangle$ be a data stream where each element e_t is drawn from a universe \mathcal{U} . The true frequency of an item $e \in \mathcal{U}$, denoted $f(e)$, is the number of times it appears in the stream: $f(e) = |\{t \mid e_t = e\}|$. The total stream length is $N = \sum_{e \in \mathcal{U}} f(e)$. CMS uses a series of scalar counters arranged in a $w \times d$ array, where each row i corresponds to a hash function h_i drawn from a pairwise independent family. The de facto standard approach defines these functions as $h_i(x) = ((a_i x + b_i) \bmod p) \bmod w$, where p is a prime number and a_i, b_i are random coefficients. When an item e arrives, CMS increments the counter at position $h_i(e)$ in each row i . The estimated frequency of an item is calculated by taking the minimum count across its hashed positions: $\hat{f}(e) = \min_{i=1}^d \text{count}[i][h_i(e)]$.

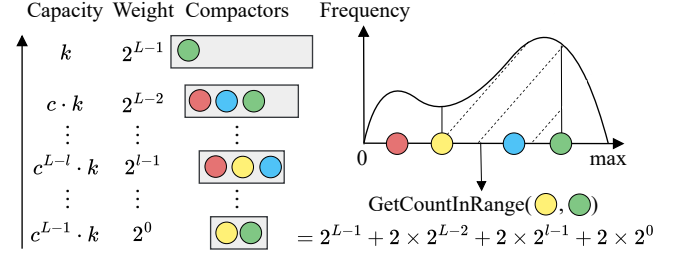


Figure 2: KLL sketch maintains multi-level compactors where items at level l have weight 2^{l-1} . The GetCountInRange operation estimates counts within any range, which generalizes both rank queries and single-item frequency estimation.

Due to hash collisions, $\hat{f}()$ can overestimate the actual count. However, by setting $d = \ln(1/\delta)$ and $w = e/\epsilon$ (where e is Euler’s constant), CMS guarantees that with probability at least $1 - \delta$, the estimated frequency satisfies $\hat{f}(e) \leq f(e) + \epsilon N$ for any item e .

Algorithm 1: KLL Quantile Sketch (q_sketch)

```
//  $k$ : Parameter controlling sketch size and accuracy
// Compactors: List of arrays storing sampled values per level
1.1 Procedure UpdateKLL(value)
1.2   Append value to the lowest level compactor (level 0)
1.3   if compactor at level 0 is full then CompactKLL(0)
1.4 Procedure QueryCountInRange(start, end)
1.5   estimated_count ← 0
1.6   for each level  $l$  do
1.7     for each value in compactor at level  $l$  do
1.8       if start < value ≤ end then estimated_count +=  $2^l$ 
1.9   return estimated_count
1.10 Procedure QueryRank(value)
1.11  return QueryCountInRange( $-\infty$ , value)
1.12 Procedure MergeKLL(other_sketch)
1.13  for each level  $l$  do
1.14    Add all items from other_sketch.Compactors[ $l$ ] to this Compactors[ $l$ ]
1.15    if compactor at level  $l$  is full then CompactKLL( $l$ )
1.16 Procedure CompactKLL( $l$ )
1.17  Sort items in Compactors[ $l$ ]
1.18  Randomly discard either the odd-indexed or even-indexed positions
1.19  Move the remaining items to the compactor at level  $l + 1$ 
1.20  if compactor at level  $l + 1$  is full then CompactKLL( $l + 1$ )
```

Quantile Summary. A quantile summary approximates the distribution of items from a totally-ordered universe \mathcal{U} . Given a stream of N items, the *rank* query of a value $e \in \mathcal{U}$, denoted $\text{Rank}(e)$, is the number of items in the stream that are less than or equal to e . A quantile query, specified by a fraction $\phi \in [0, 1]$, asks for the item e such that $\text{Rank}(e) \approx \phi N$. More generally, a quantile summary can support a $\text{QueryCountInRange}(start, end)$ that estimates the number of items falling within a specified range $(start, end]$, which generalizes rank queries.

The KLL sketch [22] is state-of-the-art, mergeable quantile summary that provides strong approximation error guarantees. It operates by maintaining a collection of L varying-capacity arrays of sampled items, called *compactors*, organized in multiple levels; although the logical height of the hierarchy grows logarithmically with the stream size, the sketch maintains a bounded number of arrays L by replacing the bottom levels with a weighted sampler when necessary. The core idea is that an item at level l has a weight of 2^{l-1} , representing exponentially more original data points than an item at a lower level, as illustrated in Figure 2. The operations

of a KLL sketch are shown in Algorithm 1. When a new item arrives, `UpdateKLL` adds it to the compactor at the lowest level (level 0). If this addition causes the compactor to exceed its capacity, a `CompactKLL` operation is triggered, which sorts the compactor, randomly samples half of the items, and "promotes" them to the next level up. This process continues until the compactor is within its capacity limits. The $\text{Rank}(e)$ of a value is estimated by summing the weights of all sampled items less than or equal to it. The accuracy and memory usage of the KLL sketch are controlled by a parameter k . For the mergeable version, setting $k = O((1/\epsilon)\sqrt{\log(1/\delta)})$ guarantees that the estimated rank is within an additive error of ϵN with probability at least $1 - \delta$, using $O(k)$ space.

Mergeability. Formally, a summarization method is considered mergeable if, given two summaries \mathcal{A}_1 and \mathcal{A}_2 computed on datasets D_1 and D_2 respectively, there exists a `Merge` operation that produces a new summary \mathcal{A}_{merged} that is valid for the union dataset $D_1 \cup D_2$ without needing to re-process the original data [2]. The merged summary \mathcal{A}_{merged} should satisfy the same guarantees as the individual summaries (e.g., same bounds ϵ, δ). Many summaries exhibit some form of mergeability. For frequency estimation, these include the Count-Min Sketch [11] and Count-Sketch [7], which require sketches to have the same width w and depth d to merge. For heavy hitter detection, counter-based algorithms like Misra-Gries [24] and SpaceSaving [23] are mergeable [2]. For quantile estimation, KLL [21] and t-digest [13] are mergeable regardless of their configured size parameters (e.g., parameter k for KLL). However, to the best of our knowledge, the resulting error bounds for merging sketches with different k parameters are not formally established; existing analysis is limited to merging sketches of identical size parameters. For membership testing, the Bloom filter [5] is also mergeable by performing a bitwise OR operation on the filter arrays.

3 PROBLEM DESCRIPTION

Let $\mathcal{A}(w, d)$ denote a $w \times d$ frequency estimation sketch (we drop (w, d) when the context does not require it). When discussing multiple sketches, we use subscripts to distinguish them (e.g., $\mathcal{A}_1, \mathcal{A}_2$). Operations on sketches are categorized into two types: (1) *Data Manipulation*: `Update`(\mathcal{A}, e) and `Query`(\mathcal{A}, e) operate on a single sketch to process items and estimate frequencies. (2) *Structure-Defining*: `Resize`, `EnhancedMerge`, and `Partition` create new sketches from existing ones, potentially changing their dimensions or combining their states. Table 2 summarizes the notations used in this paper. We now define the properties of structure-defining operations.

DEFINITION 1 (RESIZABILITY). A sketch $\mathcal{A}(w, d)$ is *resizable* if it supports the operation `Resize`(\mathcal{A}, w')¹: given $\mathcal{A}(w, d)$, this operation produces $\mathcal{A}'(w', d)$. If $w' > w$, the operation expands the sketch, resulting in an improved error bound $\epsilon' < \epsilon$. If $w' < w$, it shrinks the sketch. A sketch is truly *resizable* if w' can be any positive integer.

DEFINITION 2 (ENHANCED MERGEABILITY). A sketch supports *enhanced mergeability* if it can merge sketches of heterogeneous sizes into a new sketch of a user-defined target; i.e., the operation `EnhancedMerge`($\mathcal{A}_1, \mathcal{A}_2$) given two sketches $\mathcal{A}_1(w_1, d)$ and $\mathcal{A}_2(w_2, d)$, produces $\mathcal{A}_{merged}(w_1 + w_2, d)$, followed by a resize if $w' \neq w_1 + w_2$.

¹We use the terms `Expand` and `Shrink` when distinction between expanding ($w' > w$) and shrinking ($w' < w$) behaviors is required.

Table 2: Summary of Notations.

Symbol	Description
General Stream Notations	
S	Data stream, a sequence of items.
e_t, \mathcal{U}	An item from the item universe \mathcal{U} .
$f(e), \hat{f}(e)$	True and estimated frequency of an item e .
N	Total number of items in the stream.
KLL Sketch (Inner Sketch)	
k	Accuracy parameter controlling size and precision.
$\epsilon_{KLL}, \delta_{KLL}$	Rank error guarantee and failure probability parameters.
Compactors	Internal data structure for storing samples.
RESKETCH Notations	
\mathcal{A}, w, d	A ReSKETCH instance, its width (buckets per row), and depth (rows).
ϵ, δ	Sketch approximation and probability parameters.
seeds	An array of d unique seeds for the hash functions.
rings	An array of d consistent hash rings.
buckets	The $d \times w$ array holding the sketch's buckets.
$\text{buckets}[i][j]$	Bucket at row i , column j ; holds a counter and a q-sketch.
$\cdot.count$	The counter for items mapped to a bucket.
$\cdot.q_sketch$	The inner KLL sketch within a bucket.
Model for Mergeable, Redistributable, and Resizable Sketches	
\mathcal{A}_{id}	A sketch instance with a unique identifier id .
S_{id}	The logical stream associated with instance \mathcal{A}_{id} .
$f_{id}(e), \hat{f}_{id}(e)$	True and estimated frequency of item e in stream S_{id} .
N_{id}	The total number of items of the logical stream S_{id} .

WLOG, operations are defined for two sketches, as more sketches can be merged by successive pair-wise operations. The operation should preserve accuracy, i.e., when $w' = w_1 + w_2$, querying an item e from the resulting sketch yields accuracy comparable to the aggregated result of querying the ancestor sketches.

DEFINITION 3 (PARTITIONABILITY). A sketch is *partitionable* if it supports the operation `Partition`(\mathcal{A}, w_1, w_2): given $\mathcal{A}(w, d)$, and target widths w_1 and w_2 s.t. $w_1 + w_2 = w$, the operation produces $\mathcal{A}_1(w_1, d)$ and $\mathcal{A}_2(w_2, d)$, to operate on disjoint data subsets \mathcal{U}_1 and \mathcal{U}_2 of \mathcal{U} , while the historical state (i.e., info for frequency estimation) corresponding to any item $e \in \mathcal{U}_i$ is migrated to \mathcal{A}_i . The migration should preserve accuracy, i.e. querying an item e from its responsible sketch \mathcal{A}_i yields accuracy comparable to querying the original \mathcal{A} .

4 RESKETCH

Building upon the rationale outlined in the introduction, this section presents ReSKETCH, a frequency estimation sketch algorithmic design that achieves *resizability*, *enhanced mergeability*, and *partitionability*. We first introduce the data structure's layout. Next, we describe a core mechanism in ReSKETCH, that enables all structure-defining operations, namely, the method for redistributing bucket contents using *consistent hashing* and *quantile estimation*. After detailing the data manipulation operations, we present the structure-defining ones (`Resize`, `EnhancedMerge`, and `Partition`), along with the *partition-aware hashing* scheme to support them.

4.1 RE SKETCH Data Structure Layout

Similar to a Count-Min Sketch, ReSKETCH is built on a $d \times w$ matrix, with a “sketch of sketches” architecture, where buckets are composite structures rather than simple counters. As detailed in Table 2, each bucket contains: (1) A primary counter, $\text{buckets}[i][j].count$,

Algorithm 2: RE SKETCH – Update, Query Operations

```

// seeds[d]: Array of d unique seeds for hashing
// rings[d]: d consistent hash rings, sorted by hash point
// buckets[d][w]: 2D array of {count, q_sketch} structs

2.1 Procedure FindBucket( $e$ ,  $hash$ ,  $ring$ )
2.2   Search for first ( $p, id$ ) in  $ring$  where  $p \geq e$  hash
2.3   if no such pair found then return first  $id$  in  $ring$ 
2.4   else return  $id$ 

2.5 Procedure Update( $e$ )
2.6   for  $i \leftarrow 0$  to  $d - 1$  do
2.7      $y \leftarrow \text{Hash}(e, seeds[i])$ 
2.8      $id \leftarrow \text{FindBucket}(y, rings[i])$ 
2.9      $buckets[i][id].count += 1$ 
2.10     $buckets[i][id].q\_sketch.\text{UpdateKLL}(y)$ 

2.11 Procedure Query( $e$ )
2.12    $min\_count \leftarrow \infty$ ;  $estimates[d] \leftarrow []$ 
2.13   for  $i \leftarrow 0$  to  $d - 1$  do
2.14      $y \leftarrow \text{Hash}(e, seeds[i])$ 
2.15      $id \leftarrow \text{FindBucket}(y, rings[i])$ 
2.16      $row\_kll\_est \leftarrow buckets[i][id].q\_sketch.QueryFrequency(y)$ 
2.17      $estimates[i] \leftarrow row\_kll\_est$ 
2.18   return median( $estimates$ ) // Estimator: median of KLL estimates

```

each row correspond to the segments defined by boundary points stored in the sorted array $rings[i]$; initially, these are generated by sampling w random points from the hash space. To process an item, we determine the bucket responsible for the segment containing y using `FindBucket`, which searches the sorted boundary points in $rings[i]$ to locate the first one greater than or equal to y , i.e., the upper bound of the item's assigned segment and thus the correct bucket. The key advantage is that the pairwise-independent hash generation function `Hash` for each row remains unchanged throughout the sketch's lifetime. All structural changes, such as resizing, are handled by adjusting the segment boundaries on the ring, not by altering the hash functions. The statistical properties of this hashing scheme are analyzed in § 5.

Algorithm 3: RE SKETCH – Redistribute Row

```

3.1 Procedure RedistRow( $in\_ring$ ,  $in\_buckets$ ,  $out\_ring$ )
3.2    $out\_buckets \leftarrow$  new array of empty buckets for  $out\_ring$ 
3.3    $all\_points \leftarrow$  sorted list of unique hash points from  $in\_ring$  and  $out\_ring$ 
// Iterate through the disjoint ranges
3.4   for  $i \leftarrow 0$  to length of  $all\_points - 2$  do
3.5      $start, end \leftarrow all\_points[i], all\_points[i + 1]$ 
// For each, find its source and destination
3.6      $in\_id \leftarrow \text{FindBucket}(start, in\_ring)$ 
3.7      $out\_id \leftarrow \text{FindBucket}(start, out\_ring)$ 
3.8      $in\_bucket \leftarrow in\_buckets[in\_id]$ 
3.9      $count \leftarrow in\_bucket.q\_sketch.QueryCountInRange(start, end)$ 
3.10    if  $count > 0$  then
        // Move the data for this range to its destination
3.11     $out\_buckets[out\_id].count += count$ 
3.12     $sub\_sketch \leftarrow in\_bucket.q\_sketch.\text{FilterKLL}(start, end)$ 
3.13     $out\_buckets[out\_id].q\_sketch.\text{MergeKLL}(sub\_sketch)$ 
3.14   return  $out\_buckets$ 

```

Algorithm 4: Extended KLL Quantile Sketch (q_sketch)

```

4.1 Procedure QueryFrequency( $e$ ,  $hash$ )
4.2    $estimated\_count \leftarrow 0$ 
4.3   for each level  $l$  do
4.4     for each value in compactor at level  $l$  do
4.5       if  $value = e$  hash then  $estimated\_count += 2^l$ 
4.6   return  $estimated\_count$ 

4.7 Procedure FilterKLL( $start, end$ )
4.8    $new\_sketch \leftarrow$  new KLLSketch()
// Filter values within specified range to build new KLL
4.9   for each level  $l$  of this sketch's Compactors do
4.10    for each value in compactor at level  $l$  do
4.11      if  $start < value \leq end$  then
4.12        Add value to compactor at level  $l$  in  $new\_sketch$ 
4.13         $new\_sketch.total\_count += 2^l$ 
4.14   return  $new\_sketch$ 

```

Quantile Estimation for Count Redistribution. The role of the secondary quantile sketch is to redistribute aggregated counts when bucket boundaries are modified. As items are added via `Update`, each bucket's inner quantile sketch (q_sketch) is also updated with the item's hash value y using `UpdateKLL` to maintain a compact summary of the distribution of consistent hash values of the bucket's items. A quantile sketch enables to estimate the number of items whose hash values fall within any range ($start, end$) by using `QueryCountInRange`. When a structural change occurs (e.g., during `Resize` or `EnhancedMerge`), the segment boundaries on the consistent hash ring are modified, creating new intervals. To handle this, the function `RedistRow` (Algorithm 3) first creates a unified, sorted list of all boundary points, i.e., the union of the original and the new ring. The function then iterates through these intervals. For an interval ($start, end$), it identifies the source bucket in the old

tracking the total number of items mapped to the bucket. (2) A compact secondary quantile sketch, $buckets[i][j].q_sketch$, summarizing the distribution of hash values of the items² mapped to that bucket. For the latter, we use a KLL sketch [22] (with the same parameter k each) due to its analytical guarantees, and efficient algorithmic implementations in existing works [19].

4.2 Redistributing Bucket Contents

As discussed in the introduction, conventional sketches cannot redistribute counts during structural changes because they lack information about which items need to be moved and their individual counts. RE SKETCH addresses this through two key mechanisms: *consistent hashing* transforms bucket domains from discrete to continuous, which allows to know *which portion of items* needs to move when boundaries change (e.g., during a `Resize`); and *per-bucket quantile sketches* estimate *how many items* fall into that portion. Together, these enable bucket content redistribution for all structure-defining operations (`Resize`, `EnhancedMerge`, and `Partition`). We now describe how this redistribution works in detail.

Consistent Hashing for Bucket Selection. In the de facto standard implementations of Count-Min sketch, the pairwise independent hash functions are realized for each row i as $h_i(x) = ((a_i x + b_i) \bmod p) \bmod w$. The inner term $(a_i x + b_i) \bmod p$ generates pairwise-independent hash values in a hash space $[0, p - 1]$, while the outer term $\bmod w$ serves as a *bucket-mapping function* that reduces this range to the smaller range of sketch bucket indices $[0, w - 1]$. RE SKETCH retains the pairwise-independent hash generation but replaces the rigid outer bucket mapping function with consistent hashing [21]. This conceptually maps the generated hash values to a circular ring in each row, partitioned into w contiguous segments, each segment corresponding to a bucket in the row (illustrated in Figure 3). As shown in the `Update` operation (Algorithm 2), the hash generation call `Hash($e, seeds[i]$)` (the red highlighted line in Algorithm 7) computes $y = (a_i \cdot e + b_i \bmod p)$, which conceptually places the item on this ring. The w buckets in

²Note it keeps hash values, not items, allowing to track the distribution over the continuous hash domain, essential for redistribution, as detailed in § 4.4.

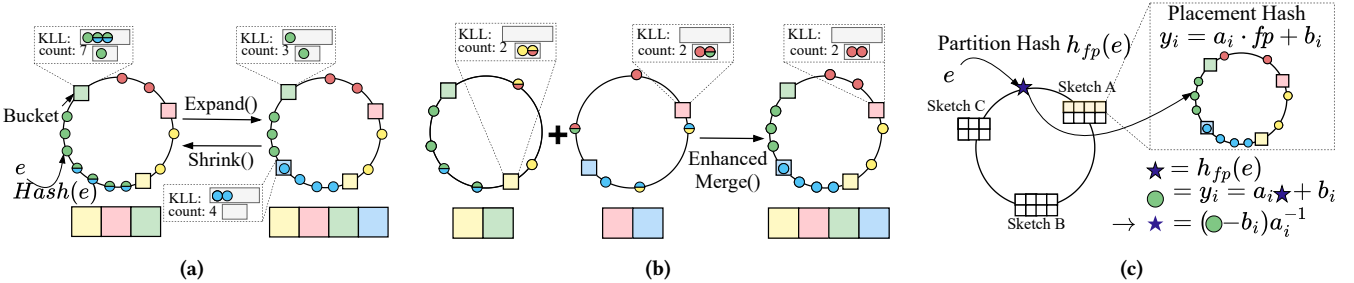


Figure 3: RE SKETCH’s structure-defining operations: (a) Resize (in form of Expand and Shrink) operations add or remove boundary points on the consistent hash ring, redistributing counts using per-bucket KLL sketches. (b) EnhancedMerge creates a unified ring with a combined width and redistributes both input sketches to the new ring structure. (c) Partition-aware hashing: item is mapped to a fingerprint via a uniform hash function $h_{fp}(e)$, then to a point on a ring via pair-wise independent placement hashing $y = a_i \cdot fp + b_i$, which determines bucket mapping. The fingerprint fp can be recovered from y through modular multiplicative inverse, therefore introducing no additional storage usage.

layout and the destination bucket in the new layout. It then queries the source bucket’s quantile sketch using `QueryCountInRange` to estimate the count of items whose hash values fall within this range. This estimate is then added to the destination bucket’s counter.

Importantly, simply transferring the count is not enough; the underlying quantile information must also be redistributed to support future operations. This is achieved in *two steps* (detailed in Algorithm 4). First, our proposed `FilterKLL` operation (line 4.7), extending the functionality of KLL creates a new, temporary KLL sub-sketch that preserves the structure of the original quantile (i.e., the same parameter k and compactor configuration), then filters the original quantile’s contents level-wise, retaining only the sampled hash values that fall within the $(start, end)$ range. Second, this new sub-sketch is combined with the destination bucket’s q_sketch using `MergeKLL`, which performs a level-wise union of the two sketches’ internal compactors and triggers compaction as needed. The entire process is visualized in Figure 3a and Figure 3b.

Properties. The redistribution operation takes $O((w+w')(\log(w+w')+k))$ steps, which can be broken down as follows: First, creating the sorted list of boundary points takes $O(w+w')$ steps, where w' is the target width. Second, the algorithm iterates through the resulting $O(w+w')$ intervals; for each, identifying the source and destination buckets using binary search takes $O(\log(w+w'))$ steps, and the quantile operations (`FilterKLL` and `MergeKLL`) perform linear scans of compactors in $O(k)$ time. The formal guarantees on the associated approximation error are provided in § 5.

4.3 Data Manipulation Operations

Update. The `Update` operation (Algorithm 2) processes an item e by updating one bucket in each row i : the item is first hashed using the pairwise-independent hash function of the row to obtain a hash value $y = (a_i \cdot e + b_i) \bmod p$ on the continuous ring (as described before, in § 4.2, regarding hashing). (Note that when Partition support is required, this is replaced by the partition-aware hashing detailed in § 4.4.) The bucket index is determined by `FindBucket($y, rings[i]$)`, through a binary search on the boundary points in $rings[i]$ to find the segment containing y . The bucket’s counter is incremented, and the hash value y is inserted into the bucket’s inner quantile sketch to update its distribution summary.

Query. The `Query` operation (Algorithm 2) leverages the distributional information stored in the inner quantile sketches to

estimate item frequency. As detailed in line 2.16, the algorithm queries the quantile sketch of each mapped bucket using KLL’s `QueryFrequency` (Algorithm 4) to obtain d independent estimates. The final estimate is the *median* of these values, since KLL estimates have two-sided errors, implying the minimum estimator (as in Count-min) is unsuitable (as it amplifies under-estimation) and, unlike the mean, the median is robust against outliers caused by heavy collisions in specific rows.

Properties. Updates take $O(d(\log w + \log k))$ steps, which accounts for d consistent hashings (i.e. $\log w$ each) and KLL updates ($O(\log k)$ each). The term $\log k$ is achieved by using the lazy compaction strategies from [19] (compared to $O(k)$ in the standard version [22]). Queries take $O(d(\log w + k))$ steps, which can be optimized to $O(d(\log w + \log k))$ for batch queries if the internal compactors are sorted beforehand. The approximation bounds for this estimator are derived in § 5.

4.4 Structure-Defining Operations

This section applies the count redistribution mechanism to implement structure-defining operations. For the EnhancedMerge and Partition, sketches must share the same hash seeds to ensure consistent mapping on the logical ring across instances, which allows their structures to be combined or partitioned meaningfully.

Resize. The `Resize` operation (Algorithm 5) adjusts the row width from w to w' . It first calculates the difference $\Delta = w' - w$ to update the consistent hashing ring structure for each row. If $\Delta > 0$ (expansion), Δ new boundary points are randomly added to the ring to increase granularity; if $\Delta < 0$ (shrinking), $|\Delta|$ boundary points are randomly removed, which merges adjacent segments (illustrated in Figure 3a). Once the ring is updated, the function invokes `RedistRow` on each row to transfer frequencies and quantile summaries from the old bucket array to the new one.

Algorithm 5: RE SKETCH – Resize Operation

```

5.1 Procedure Resize( $\mathcal{A}, w'$ )
5.2    $\mathcal{A}.buckets \leftarrow$  new bucket array of size  $\mathcal{A}.d \times w'$ ;  $\Delta \leftarrow w' - \mathcal{A}.w$ 
5.3   for  $i \leftarrow 0$  to  $\mathcal{A}.d - 1$  do
5.4      $out\_ring \leftarrow \mathcal{A}.rings[i]$ 
5.5     if  $\Delta > 0$  then Add  $\Delta$  random points to  $out\_ring$ 
5.6     else Remove  $|\Delta|$  random points from  $out\_ring$ 
5.7      $\mathcal{A}.buckets[i] \leftarrow \text{RedistRow}(\mathcal{A}.rings[i], \mathcal{A}.buckets[i], out\_ring)$ 
5.8      $\mathcal{A}.rings[i] \leftarrow out\_ring$ ;
5.9    $\mathcal{A}.buckets \leftarrow \mathcal{A}.buckets$ ;  $\mathcal{A}.w \leftarrow w'$ 
```

435 **Enhanced Merge.** The EnhancedMerge operation (Algorithm 6)
 436 combines two sketches $\mathcal{A}_1(w_1, d)$ and $\mathcal{A}_2(w_2, d)$ into $\mathcal{A}_{merged}(w_1 +$
 437 $w_2, d)$. First, a new merged_sketch is initialized. For each row,
 438 its ring is formed by the union of the points from the rings of
 439 \mathcal{A}_1 and \mathcal{A}_2 (Figure 3b illustrates this process). Then, for each of
 440 the original sketches, RedistRow redistributes its contents into
 441 temporary bucket arrays that conform to the new merged ring
 442 layout. Finally, the function iterates through the new buckets, and
 443 aggregates the results by summing the primary counters and calling
 444 MergeKLL on the quantile sketches element-wise. To merge more
 445 sketches, EnhancedMerge can be generalized by creating a new ring
 446 in each row with the union of the boundaries from all sketches;
 447 alternatively, it can be called iteratively to merge them pairwise,
 until all are combined into one.

Algorithm 6: REsketch – Merge Operation

```

6.1 Procedure EnhancedMerge( $\mathcal{A}_1, \mathcal{A}_2$ )
6.2    $new\_width \leftarrow \mathcal{A}_1.w + \mathcal{A}_2.w$ 
6.3    $\mathcal{A}_{merged} \leftarrow$  new REsketch( $\mathcal{A}_1.d, new\_width, \mathcal{A}_1.seeds$ )
6.4   for  $i \leftarrow 0$  to  $\mathcal{A}_1.d - 1$  do
6.5      $T1 \leftarrow$  RedistRow( $\mathcal{A}_1.rings[i], \mathcal{A}_1.buckets[i], \mathcal{A}_{merged}.rings[i]$ )
6.6      $T2 \leftarrow$  RedistRow( $\mathcal{A}_2.rings[i], \mathcal{A}_2.buckets[i], \mathcal{A}_{merged}.rings[i]$ )
6.7     for  $j \leftarrow 0$  to  $new\_width - 1$  do
6.8        $\mathcal{A}_{merged} \leftarrow \mathcal{A}_{merged}.buckets[i][j]$ 
6.9        $\mathcal{A}_{merged}.count \leftarrow T1[j].count + T2[j].count$ 
6.10       $\mathcal{A}_{merged}.q\_sketch \leftarrow T1[j].q\_sketch$ 
6.11       $\mathcal{A}_{merged}.q\_sketch.MergeKLL(T2[j].q\_sketch)$ 
6.12   return  $\mathcal{A}_{merged}$ 

```

448 **Partition.** The Partition operation (Algorithm 7) splits $\mathcal{A}(w, d)$
 449 into two smaller, separate instances $\mathcal{A}_1(w_1, d)$ and $\mathcal{A}_2(w_2, d)$ (where
 450 $w_1 + w_2 = w$). A naive approach might simply split the bucket array
 451 of each row at index w_1 . However, as established in Algorithm 2,
 452 the hash value generation is pairwise-independent; therefore, an
 453 item e might map to one of the first w_1 buckets in one row and to
 454 one of the subsequent w_2 buckets in another row. Consequently,
 455 future updates or queries for e would need to be sent to both in-
 456 stances, which would undermine the purpose of partitioning in
 457 distributed processing. To address this, we introduce **Partition-**
 458 **Aware Hashing** (highlighted in green in Algorithm 7, visualized
 459 in Figure 3c), which replaces the standard pairwise-independent
 460 hashing (highlighted in red).

461 This technique treats hash value generation as a composition
 462 of two steps: **1 Partition Hashing:** The item e is mapped to a
 463 fingerprint fp via a uniform partition hash function $h_{fp}(e)$. This
 464 fingerprint acts as an immutable identifier for the item's partition
 465 assignment for its entire lifetime. **2 Placement Hashing:** The
 466 pairwise-independent transformation for row i then operates on
 467 this fingerprint: $y = a_i \cdot fp + b_i$ rather than on the raw item (see
 468 Figure 3c). The reasoning of this 2-step process is analogous to
 469 how Resize relies on slicing the continuous bucket ring to redis-
 470 tribute items between buckets; i.e., partitioning relies on slicing
 471 the continuous fingerprint domain to redistribute items between
 472 sketches, which allows partitioned sketches to be partitioned fur-
 473 ther or merged similarly.

474 To enable state migration during a Partition, the fingerprint fp
 475 must be recoverable from the hash values stored within the sketch's
 476 buckets; otherwise, we would need to store the fingerprint alongside
 477 every hash value, which would double the space needs. However,
 478 since the hash value is the result of a modulo operation ($\text{mod } p$),

Algorithm 7: REsketch – Partition Operation

```

7.1 Procedure Hash( $e, seed_i$ )
7.2   return  $seed_i.a \cdot e + seed_i.b$  // Original 2-wise independent hash
7.3   // Partition-aware hashing; replaces the original hash logic
7.4   when Partition is supported
7.5      $fp \leftarrow h_{fp}(e)$  // Step 1: Partition (uniform) Hash
7.6     return  $seed_i.a \cdot fp + seed_i.b$  // Step 2: Placement (2-indep.) Hash
7.7 Procedure ModInverse( $a$ )
7.8   return  $a^{-1}$  //  $(a \cdot a^{-1}) \bmod 2^W = 1$ , where  $W$  is word width
7.9 Procedure RecoverFingerprint( $y, seed_i$ )
7.10   //  $y = seed_i.a \cdot fp + seed_i.b \implies fp = (y - seed_i.b) \cdot a_{seed_i.a}^{-1}$ 
7.11   return  $(y - seed_i.b) \cdot \text{ModInverse}(seed_i.a)$ 
7.12 Procedure Partition( $\mathcal{A}, w_1, w_2$ )
7.13    $\mathcal{A}_1 \leftarrow$  new REsketch( $\mathcal{A}.d, w_1, \mathcal{A}.seeds$ )
7.14    $\mathcal{A}_2 \leftarrow$  new REsketch( $\mathcal{A}.d, w_2, \mathcal{A}.seeds$ )
7.15   // Define split_point on the primary partition space [0, 1)
7.16    $split\_point \leftarrow w_1 / (w_1 + w_2)$ 
7.17   foreach  $(i, y, weight)$  in  $\mathcal{A}$  do
7.18      $fp \leftarrow$  RecoverFingerprint( $y, \mathcal{A}.seeds[i]$ )
7.19     if  $fp < split\_point$  then Reinsert( $\mathcal{A}_1, i, y, weight$ )
    else Reinsert( $\mathcal{A}_2, i, y, weight$ )
7.20   return  $\mathcal{A}_1, \mathcal{A}_2$ 
7.21 Procedure Reinsert( $\mathcal{A}, i, y, weight$ )
7.22   Add weighted sample  $(y, weight)$  to the correct bucket in row  $i$  of  $\mathcal{A}$ 

```

multiple fingerprints can map to the same hash value, hence cannot
 480 be uniquely recovered. To do this on W -bit registers, we can map the
 481 fingerprint to a general finite field $\text{GF}(2^W)$ and perform arithmetic
 482 operations (i.e., $a_i \cdot fp + b_i$) in this field [25]. In this domain, the
 483 linear transformation $a_i x + b_i$ is a bijection for all $a_i \neq 0$, which
 484 can allow to always recover the fingerprint from the hash value.
 485 Partition employs this to split the sketch based on a split point
 486 in the partition space. As shown in Algorithm 7, it iterates through
 487 all summarized samples, recovers fp to determine which of the two
 488 new sketches the sample belongs to, and re-inserts the samples and
 489 their weights accordingly.

Practical Implementation of Partition-Aware Hashing

Arithmetic in $\text{GF}(2^W)$ is computationally expensive in commodity hardware, as it requires polynomial multiplication and modular reductions. Consequently, we adopt a more efficient approach that leverages the native 2's complement representation integer arithmetic of modern processors (e.g., x86). We treat the fingerprint fp and hash values as standard W -bit machine words (e.g., $W = 64$), and apply the linear transformation $y = a_i \cdot fp + b_i$, constrained that a_i is odd, without an explicit modulo p operation. Figure 3c illustrates this hashing mechanism. On W -bit registers, multiplication automatically discards overflow bits, which is equivalent to performing operations modulo 2^W . This guarantees both statistical uniformity and reversibility. Regarding uniformity, we rely on Fact 3.4 from Thorup [33], which states that for any modulus m and multiplier a coprime to m , the linear map $x \mapsto ax + b \pmod{m}$ preserves the uniform distribution of the input. Due to the fact that fp is uniformly distributed, and our multiplier a_i is odd (coprime to 2^W), the resulting hash values are uniform over the ring. Regarding reversibility, also because a_i is coprime to 2^W , a multiplicative inverse a_i^{-1} is guaranteed to exist. This allows us to recover the original fingerprint fp from a stored hash value y via the operation $fp = (y - b_i) \cdot a_i^{-1} \pmod{2^W}$.

Time Complexity. The cost of Resize is determined by the cost of RedistRow across d rows, which is $O(d(w+w')(\log(w+w')+k))$. For EnhancedMerge, the complexity consists of the redistribution overhead for the input sketches plus the cost of merging the resulting buckets. Since merging two KLL sketches takes $O(k)$ [22]

497 steps, the additional merging cost is $O(d(w_1 + w_2)k)$. Adding this
 498 to the redistribution cost yields a total complexity of $O(d((w_1 +$
 499 $w_2) \log(w_1 + w_2) + k))$. Finally, Partition involves iterating over
 500 every sample stored in the sketch to recover its fingerprint and
 501 re-insert it. With $d \times w$ buckets each storing $O(k)$ items, and consider-
 502 ing that re-inserting each item requires finding the target bucket
 503 in $O(\log w)$ and adding it as a weighted sample in $O(1)$, this opera-
 504 tion has a total time complexity of $O(dwk \log w)$.

5 RESKETCH ANALYSIS

505 In this section, we analyze ReSKETCH’s frequency estimation ap-
 506 proximation bounds. We begin in § 5.1 by establishing the bound for
 507 a static single sketch and then extend to dynamic and distributed
 508 cases in § 5.2, where sketches undergo structure-defining opera-
 509 tions. Towards the latter, we introduce an *instance provenance* graph
 510 to track error accumulation across operations, analyze errors from
 511 both data processing and structure-defining operations, and derive
 512 our main theorem (Theorem 15), which provides a bound for any
 513 sketch instance produced by an arbitrary sequence of operations.

5.1 Static Single REsketch Bound

514 We first analyze the expected bucket load in ReSKETCH’s consistent
 515 hashing scheme. Let $C^{i,j}$ denote the count in bucket j of row i .

516 **LEMMA 4 (EXPECTED BUCKET LOAD).** *For a static $\mathcal{A}(w, d)$ process-
 517 ing a stream of length N , given any arbitrary item e , the expected
 518 count in row i bucket j , where j is the bucket that e is hashed to for
 519 row i , is $\mathbb{E}[C^{i,j}] \approx \frac{2N}{w}$.*

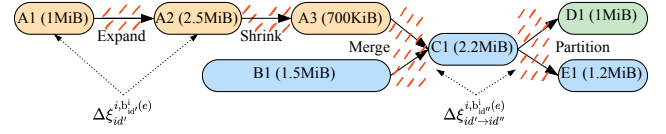
520 **PROOF.** The placement of w random bucket boundaries and one
 521 specific item’s hash value on the ring, partitions it into $w + 1$ in-
 522 tervals, each with expected length $\frac{1}{w+1}$ by uniformity. The bucket
 523 containing e consists of the interval between the boundary preced-
 524 ing e ’s hash value and the one succeeding it. Thus, its expected
 525 length is $\frac{2}{w+1} \approx \frac{2}{w}$, and the expected count is $\frac{2N}{w}$. □

526 **LEMMA 5 (KLL FREQUENCY ESTIMATION ERROR).** *Consider a KLL
 527 sketch with parameter k , that processed N items. Define the estimated
 528 frequency of an item e as $\hat{f}(e) = \text{rank}(e) - \text{rank}(e^-)$, where e^-
 529 denotes the value immediately preceding e in the totally-ordered
 530 domain. Then, $|\hat{f}(e) - f(e)| \leq 2\epsilon_{KLL} \cdot N$ with probability at least
 531 $1 - \delta_{KLL}$ for any item e , where $f(e)$ is the true frequency.*

532 **PROOF.** A KLL sketch provides rank queries with error at most
 533 $\epsilon_{KLL} \cdot N$ with probability at least $1 - \delta_{KLL}$. Since both rank queries
 534 contribute at most $\pm \epsilon_{KLL} \cdot N$ error, the total error satisfies $|\hat{f}(e) -$
 535 $f(e)| \leq 2\epsilon_{KLL} \cdot N$ with probability at least $1 - \delta_{KLL}$. □

536 **LEMMA 6 (MEDIAN AMPLIFICATION).** *Consider estimating the
 537 frequency $f(e)$ of a specific item e using d independent estima-
 538 tors. Suppose each estimator fails to satisfy an approximation bound
 539 $|\hat{f}(i)e - f(e)| \leq \epsilon$ with probability at most $p < 1/2$. Then, the median
 540 of these estimators fails to satisfy the same bound with probability at
 541 most δ , provided $d = O(\log(1/\delta))$.*

542 **PROOF.** Let X_i be the indicator random variable that estimator i
 543 fails, and let $X = \sum_{i=1}^d X_i$. The median fails if and only if at least
 544 $d/2$ estimators fail, i.e., $X \geq d/2$. We have $\mathbb{E}[X] = p \cdot d < d/2$.



545 **Figure 4: Instance provenance DAG illustrating error tracking across**
 546 **operations.** Each node represents a sketch instance with its size, also
 547 represents data processing period with error reference $\xi_{id'}^{i,b}_i(e)$; solid
 548 edges represent structure-defining operations with error reference
 549 $\xi_{id' \rightarrow id''}^{i,b}_i(e)$. Error accumulation follows provenance paths to \mathcal{A}_{id} (e.g.,
 550 \mathcal{A}_{C1} inherits errors from $\mathcal{A}_{A1} \rightarrow \mathcal{A}_{A2} \rightarrow \mathcal{A}_{A3}$ and \mathcal{A}_{B1}). □

551 By the Chernoff bound, $\Pr[X \geq d/2] = \exp(-\Theta(d))$. Setting $d =$
 552 $O(\log(1/\delta))$ ensures the failure probability is at most δ . □

553 **THEOREM 7 (STATIC SINGLE REsketch ERROR BOUND).** *For a*
 554 *static $\mathcal{A}(w, d)$ processing a stream of length N , the estimate satisfies*
 555 $|\hat{f}(e) - f(e)| \leq \epsilon N$ *with probability $\geq 1 - \delta$ using space $O\left(\frac{1}{\epsilon} \log \frac{1}{\delta}\right)$.* □

556 **PROOF.** Let $C^{i,j}$ denote the count in e ’s bucket in row i . By
 557 Lemma 4, $\mathbb{E}[C^{i,j}] \approx 2N/w$. The row- i estimate fails if either (1) the
 558 KLL fails internally (prob. $\leq \delta_{KLL}$), or (2) the bucket load satisfies
 559 $2\epsilon_{KLL} \cdot C^{i,j} > \epsilon N$ (the factor 2 follows from Lemma 5). By Markov,
 560 $\Pr[(2)] \leq \frac{2\epsilon_{KLL} \cdot 2N/w}{\epsilon N} = \frac{4\epsilon_{KLL}}{\epsilon w}$, so $P_{\text{row_fail}} \leq \delta_{KLL} + \frac{4\epsilon_{KLL}}{\epsilon w}$. □

561 The final estimator takes the median of d independent row es-
 562 timates. To apply Lemma 6, we require $P_{\text{row_fail}} < 1/2$. Let’s choose
 563 $P_{\text{row_fail}} \leq 1/3$, and allocate the budget evenly: set $\delta_{KLL} = 1/6$
 564 for event (1), and $w = 24\epsilon_{KLL}/\epsilon$ for event (2). By Lemma 6 with
 565 $d = O(\log(1/\delta))$, the median fails with probability $\leq \delta$. □

566 The space is $d \times w \times k$, where each bucket stores one KLL of
 567 the same size $O(k)$. Since $k = O(1/\epsilon_{KLL})$ for fixed $\delta_{KLL} = 1/6$, we
 568 have: Space = $d \cdot w \cdot k = O(\log \frac{1}{\delta}) \cdot \frac{24\epsilon_{KLL}}{\epsilon} \cdot \frac{1}{\epsilon_{KLL}} = O(\frac{1}{\epsilon} \log \frac{1}{\delta})$. □

5.2 Dynamic Distributed REsketch Bound

569 Theorem 7 bounds approximation errors for a single sketch instance
 570 at fixed width. However, dynamic (distributed or parallel) systems
 571 have multiple sketch origins processing different streams and un-
 572 dergoing structure-defining operations (Resize, EnhancedMerge,
 573 Partition). Therefore, the error bound must account for: (a) data
 574 processing across multiple instances, each potentially at different
 575 widths, (b) errors introduced by structure-defining operations (c) er-
 576 rors persisted from prior operations. □

577 To reason about error accumulation in such systems, we formalize
 578 sketch instances and their relationships. Each *sketch instance*,
 579 denoted \mathcal{A}_{id} with a unique identifier id , conceptually summarizes a
 580 *logical stream*, S_{id} , the conceptual multiset of all items it processed,
 581 with a total number of items denoted N_{id} . This logical stream in-
 582 cludes both items directly processed by the instance and items
 583 inherited from ancestor instances through the provenance paths,
 584 which will be defined shortly. For example, when two instances \mathcal{A}_1
 585 and \mathcal{A}_2 merge to create $\mathcal{A}_{\text{merged}}$, the logical stream summarized
 586 by the merged sketch, S_{merged} , contains all items from both S_1 and
 587 S_2 , and thus $N_{\text{merged}} = N_1 + N_2$. The relationships between sketch
 588 instances form a directed acyclic graph (DAG) defined as follows:

589 **DEFINITION 8 (INSTANCE PROVENANCE DAG).** *The instance prove-*
 590 *nance DAG (example illustrated in Figure 4) is a directed acyclic graph* □

588 where: (i) Nodes and processing periods: Each node represents a
 589 sketch instance \mathcal{A}_{id} with an associated logical stream, i.e., the sub-
 590 stream of data items it processes. A processing period is an interval
 591 during which a sketch instance processes updates (also represented as
 592 part of the respective node of the graph). (ii) Edges represent struc-
 593 ture-defining operations (Resize, EnhancedMerge, or Partition) that
 594 create descendant instances from ancestors. For a given sketch instance
 595 \mathcal{A}_{id} , consider the provenance paths originating from source nodes
 596 (i.e., sketch instances with no predecessors) and terminating at \mathcal{A}_{id} .
 597 Based on them, define: (iii) \mathcal{P}_{id} : The set of all sketch instance IDs along
 598 those provenance paths. (iv) \mathcal{Q}_{id} : The set of all structure-defining
 599 transitions $id' \rightarrow id''$ occurring along these paths.

600 Unlike the static single sketch case, where an item is always
 601 mapped to the same bucket j in each row and bucket count $C_{id}^{i,j}$
 602 increases monotonically, structure-defining operations can move
 603 items between buckets, which may alter the bucket index for item
 604 e and cause bucket counts to both increase and decrease. Let $b_{id}^i(e)$
 605 be the index of the bucket in row i to which item e maps in the
 606 analyzed instance \mathcal{A}_{id} . We denote by $C_{id}^{i,b_{id}^i(e)}$ the total item count
 607 within this bucket in row i .

608 Bucket counts change through two types of operations: (1) *Data*
 609 *processing at instance id*: The change is denoted $\Delta C_{id}^{i,b_{id}^i(e)}$, which
 610 represents items added to instance id during data processing pe-
 611 riod. The subscript id alone indicates processing happening at this
 612 instance. (2) *Structure-defining operation id $\rightarrow id'$* : The change is
 613 denoted $\Delta C_{id \rightarrow id'}^{i,b_{id'}^i(e)}$, which represents bucket changes during the
 614 transformation from instance id to id' . The subscript $id \rightarrow id'$
 615 indicates a transition between instances. $\Delta C_{id}^{i,b_{id}^i(e)}$ and $\Delta C_{id \rightarrow id'}^{i,b_{id'}^i(e)}$
 616 do not directly bound the error increment because KLL compaction
 617 errors are irreversible. KLL error arises from compaction: as more
 618 items are processed, more compaction occurs, which creates er-
 619 ror. For example, Expand may reduce the bucket count ($\Delta C_{id \rightarrow id'}^{i,b_{id'}^i(e)} < 0$), but prior compaction errors from items already compacted can-
 620 not be recovered. We introduce an *error reference variable* $\xi_{id}^{i,b_{id}^i(e)}$
 621 which accounts for the fact that only operations increasing bucket
 622 count cause new compaction.

624 **DEFINITION 9 (ERROR REFERENCE VARIABLE).** For item e in row
 625 i , we define the incremental error reference variable $\xi_{id}^{i,b_{id}^i(e)}$ for
 626 each operation or processing period. The cumulative error reference
 627 for item e in row i at instance \mathcal{A}_{id} , denoted $\Xi_{id}^{i,b_{id}^i(e)}$ is the sum of
 628 all incremental error contributions along the provenance paths from
 629 source nodes to id :

$$\Xi_{id}^{i,b_{id}^i(e)} = \sum_{id' \in \mathcal{P}_{id}} \xi_{id'}^{i,b_{id'}^i(e)} + \sum_{id' \rightarrow id'' \in \mathcal{Q}_{id}} \xi_{id' \rightarrow id''}^{i,b_{id''}^i(e)}$$

630 *Remark.* The following lemmas show that the accuracy requirements
 631 in Definitions 1, 2, and 3 are met. Due to space constraints, we provide
 632 their proofs in the extended version [26].

633 **LEMMA 10 (DATA PROCESSING ERROR REFERENCE).** Consider data
 634 processing at $\mathcal{A}_{id}(w_{id}, d)$ that processes ΔN_{id} items. For any item e
 635 in any row i , the incremental error reference satisfies: $\mathbb{E}[\xi_{id}^{i,b_{id}^i(e)}] =$
 636 $2\Delta N_{id}/w_{id}$.

637 **LEMMA 11 (EXPAND ERROR REFERENCE).** Consider the Resize op-
 638 eration from $\mathcal{A}_{id}(w, d)$ to $\mathcal{A}_{id'}(w' > w, d)$, i.e., expanding the sketch.
 639 For any item e in any row i , the operation introduces no additional
 640 error reference: $\xi_{id \rightarrow id'}^{i,b_{id'}^i(e)} = 0$.

641 **LEMMA 12 (SHRINK ERROR REFERENCE).** Consider the Resize oper-
 642 ation from $\mathcal{A}_{id}(w, d)$ to $\mathcal{A}_{id'}(w' < w, d)$, i.e., shrinking the sketch,
 643 where N_{id} is the total number of items processed by \mathcal{A}_{id} before the
 644 resize. For any item e in any row i , the incremental error reference
 645 satisfies: $\mathbb{E}[\xi_{id \rightarrow id'}^{i,b_{id'}^i(e)}] = \mathbb{E}[\Delta C_{id \rightarrow id'}^{i,b_{id'}^i(e)}] = 2N_{id}(1/w' - 1/w)$.

646 **LEMMA 13 (ENHANCED MERGE ERROR REFERENCE).** Consider the
 647 EnhancedMerge operation combining $\mathcal{A}_1(w_1, d)$ and $\mathcal{A}_2(w_2, d)$ into
 648 $\mathcal{A}_{id'}(w_1 + w_2, d)$. For any item e in any row i , the operation introduces
 649 no additional expected error reference: $\mathbb{E}[\xi_{(id_1, id_2) \rightarrow id'}^{i,b_{id'}^i(e)}] = 0$.

650 **LEMMA 14 (PARTITION ERROR REFERENCE).** Consider the Partition
 651 operation of $\mathcal{A}_{id}(w, d)$ into $\mathcal{A}_1(w_1, d)$ and $\mathcal{A}_2(w_2, d)$, where $w_1 + w_2 =$
 652 w . For any item e in any row i , the operation introduces no additional
 653 expected error reference: $\mathbb{E}[\xi_{id \rightarrow (id_1, id_2)}^{i,b_{id'}^i(e)}] = 0$.

654 **THEOREM 15 (DYNAMIC DISTRIBUTED RESKETCH ERROR BOUND).**
 655 For $\mathcal{A}_{id}(w, d)$ processing a total stream length $N_{id} = \sum_{id' \in \mathcal{P}_{id}} \Delta N_{id'}$,
 656 the frequency estimate satisfies $|\hat{f}(e) - f(e)| \leq \varepsilon N_{id}$ with probability
 657 $\geq 1 - \delta$, provided:

$$\sum_{id' \in \mathcal{P}_{id}} \frac{\Delta N_{id'}}{w_{id'}} + \sum_{(id' \rightarrow id'') \in \mathcal{Q}_{id}} N_{id'} \left(\frac{1}{w_{id''}} - \frac{1}{w_{id'}} \right) \leq \frac{\varepsilon N_{id}}{24\varepsilon_{KLL}}$$

658 **PROOF.** For row i , by Lemma 5, the KLL sketch satisfies $|\hat{f}_i(e) -$
 659 $f(e)| \leq 2\varepsilon_{KLL} \cdot \Xi_{id}^{i,b_{id}^i(e)}$ with probability $1 - \delta_{KLL}$, where $\Xi_{id}^{i,b_{id}^i(e)}$
 660 serves as stream length for the KLL in that bucket. By Definition 9,
 661 and Lemmas 10–14, we have: $\mathbb{E}[\Xi_{id}^{i,b_{id}^i(e)}] = \sum_{id' \in \mathcal{P}_{id}} \frac{2\Delta N_{id'}}{w_{id'}} +$
 662 $\sum_{(id' \rightarrow id'') \in \mathcal{Q}_{id}} \left(\frac{2N_{id'}}{w_{id''}} - \frac{2N_{id'}}{w_{id'}} \right)$.
 663 **is Shrink**

664 The row- i estimate fails if either: (1) The KLL fails internally with
 665 probability $\leq \delta_{KLL}$, or (2) The cumulative error $2\varepsilon_{KLL} \cdot \Xi_{id}^{i,b_{id}^i(e)}$ ex-
 666 ceeds εN_{id} . By Markov's inequality, $\Pr[2\varepsilon_{KLL} \cdot \Xi_{id}^{i,b_{id}^i(e)} \geq \varepsilon N_{id}] \leq$
 667 $\frac{2\varepsilon_{KLL} \cdot \mathbb{E}[\Xi_{id}^{i,b_{id}^i(e)}]}{\varepsilon N_{id}}$. Let X be the left-hand side of the condition in-
 668 equality. Then $\mathbb{E}[\Xi_{id}^{i,b_{id}^i(e)}] = 2X$. Substituting $X \leq \frac{\varepsilon N_{id}}{24\varepsilon_{KLL}}$, we
 669 get: $\Pr[(2)] \leq \frac{2\varepsilon_{KLL} \cdot 2(\frac{\varepsilon N_{id}}{24\varepsilon_{KLL}})}{\varepsilon N_{id}} = \frac{4\varepsilon_{KLL} \cdot \varepsilon N_{id}}{24\varepsilon_{KLL} \cdot \varepsilon N_{id}} = \frac{1}{6}$. Thus, $P_{\text{row_fail}} \leq$
 670 $\delta_{KLL} + 1/6$. Setting $\delta_{KLL} = 1/6$ gives $P_{\text{row_fail}} \leq 1/3$. Taking the
 671 median of $d = O(\log(1/\delta))$ independent row estimates, Lemma 6
 ensures the estimate succeeds with probability $\geq 1 - \delta$. \square

672 This theorem provides two practical implications: First, it serves
 673 as a verification mechanism: given an initial target error bound ε ,
 674 one can verify if the guarantee holds after an arbitrary sequence
 675 of operations by checking if the cumulative errors (the left-hand
 676 side of the inequality) remain below the derived threshold. Second,
 677 it enables dynamic bound derivation: e.g., in cases where the se-
 678 quence of shrinking operations forces the sketch error go beyond
 679 its original parameters, the inequality can be inverted to find the
 680 new effective error. This allows the system to quantify the accuracy
 681 trade-offs incurred by dynamic resizing, merging, and partitioning.

682 6 EVALUATION

683 Here, we provide an evaluation of the performance of ReSKETCH
 684 in three parts. First, a *sensitivity analysis* is performed, both to as-
 685 sociate the performance of RESENCH with the bounds in the anal-
 686 ysis, and to select suitable parameters for subsequent benchmarks.
 687 Second, we perform *benchmarks of the operations* supported by RE-
 688 SKETCH: Update, Query, Resize, EnhancedMerge, and Partition. Third,
 689 based on the example application from § 1, we demonstrate the
 690 benefits enabled by RESENCH in a *realistic network monitoring* sce-
 691 nario. To begin, we describe the evaluation environment, datasets,
 692 baselines, and parameters. After presenting detailed benchmark
 693 results, we summarize the main takeaways.

694 *Environment.* All experiments are conducted on an Intel Xeon
 695 E5-2695 v4 processor running at 2.1 GHz with three-level cache
 696 hierarchy (32 KiB L1, 256 KiB L2, and 45 MiB L3). RESENCH and
 697 baselines are implemented in C++³, compiled with GCC 15.2.1 using
 698 -O3 on openSUSE Tumbleweed 20251127. All data are averages over
 699 30 runs, with shaded regions illustrating run-to-run variance.

700 *Dataset.* We use the CAIDA Anonymized Internet Traces 2018 [6],
 701 a broadly used benchmark in network monitoring literature [31, 36,
 702 37]. We extract source IP addresses from the first 10 M packets, rep-
 703 resenting network traffic monitoring scenarios with realistic skew-
 704 ness that is commonly observed in real-world environments [12].

705 *Baselines.* The performance of RESENCH is evaluated relative to:
 706 (1) Count-Min Sketch (CMS), as described in § 2, an efficient, estab-
 707 lished sketch, however lacking support for resizing and enhanced
 708 mergeability. (2) Dynamic Count-Min Sketch (DCMS) [38], a design
 709 for coarse-grained expansion using an ever-growing linked list of
 710 complete CMS instances in order to maintain certain estimation
 711 error bounds for skewed data, but does not support shrinking to
 712 reclaim memory. (3) Geometric Sketch (GS) [4], which supports
 713 fine-grained dynamic resizing in both directions; however, it cannot
 714 shrink below its initial allocation. As noted, no prior work supports
 715 enhanced merging and the ability to adjust partitioning.

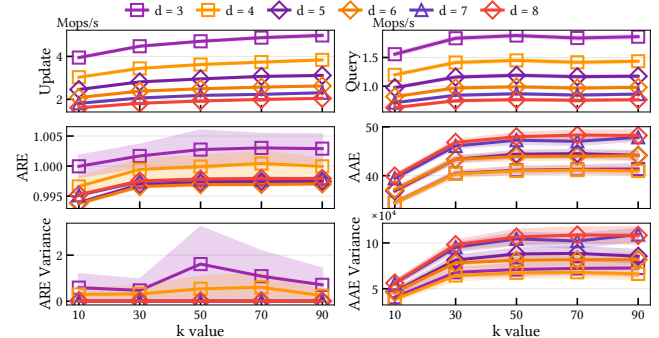
716 *Hashing.* We use 64-bit xxHash [8] for partition hashing $h_{fp}(e)$
 717 (§ 6.12), due to its high throughput on small inputs and good quality
 718 regarding collisions and random dispersion of hash values [34].

719 *Metrics of interest.* We evaluate several metrics, defined as fol-
 720 lows: (1) *Update Throughput* measures the number of processed
 721 items per second. (2) *Query throughput* measures the number of
 722 queries processed per second. (3) *Memory usage* measures the
 723 space needed for data structures. (4) *Average Relative Error (ARE)*
 724 ($\frac{1}{|S|} \sum_{e \in S} \frac{|f(e) - \hat{f}(e)|}{f(e)}$) measures the deviation between true and
 725 estimated frequencies across all distinct items in S . (5) *Average Ab-
 726 solute Error (AAE)* ($\frac{1}{|S|} \sum_{e \in S} |f(e) - \hat{f}(e)|$) similarly measures the
 727 absolute deviation between true and estimated frequencies. (6) *ARE*
 728 *variance* ($\frac{1}{|S|} \sum_{e \in S} (\frac{|f(e) - \hat{f}(e)|}{f(e)} - \text{ARE})^2$) measures the dispersion
 729 of relative errors across items within a single run. (7) *AAE variance*
 730 ($\frac{1}{|S|} \sum_{e \in S} (|f(e) - \hat{f}(e)| - \text{AAE})^2$) measures the dispersion of ab-
 731 solute errors across items within a single run. The variance metrics
 732 are designed to measure the dispersion of relative and absolute
 733 errors across all items in the sketch, testing the stability of the
 734 returned estimates; i.e. large errors for a few keys will weigh more

735 than small errors for many keys, a behavior that ARE/AAE cannot
 736 reveal due to taking the mean.

737 *Parameters.* To evaluate RESENCH, the parameters k , d , and w
 738 (as in Table 2) need to be configured. The total memory M of the
 739 structure is given by $d \cdot w \cdot 3k$, where $3k$ is the upper bound on the
 740 size of a KLL with parameter k . To this end, we perform a sensitivity
 741 analysis to select suitable parameters for subsequent benchmarks.

742 6.1 Sensitivity Analysis



743 **Figure 5: Varying k and d (rows) for RESENCH with fixed $M = 64$ KiB.**

744 *Method.* Using different memory budgets $M = 32, 64, 256$ and
 745 1024 KiB, we process 10 M items from the CAIDA dataset with var-
 746 ious combinations of k and d , setting w accordingly to satisfy the
 747 chosen M . For brevity, we show results for $M = 64$ KiB here, while
 748 the remaining figures can be found alongside the implementation,
 749 in the open repository [26]. Values of M are chosen based on the
 750 memory needed to count all unique items in the input dataset accu-
 751 rately; there are 154 k unique items, requiring $154000 \cdot 24 \approx 1203$ KiB
 752 – this is the upper bound on M . We explore the performance of
 753 these parameter choices on the aforementioned metrics: through-
 754 put for update and query operations, accuracy measured as ARE
 755 and AAE, and the within-run variance of each.

755 *Results.* Results for all 6 metrics are shown in Figure 5. Through-
 756 put decreases with increasing d as each additional row requires
 757 an additional row update/read operation. Increasing k for fixed d
 758 shows improved throughput for updates, as larger capacity com-
 759 pactors perform compaction operations less frequently. Impact of
 760 k on query throughput is less significant, as queries take a similar
 761 amount of time regardless of w . ARE with few rows ($d = 3$ or 4)
 762 is higher than for deeper sketches, as the median estimator has
 763 fewer input estimators to sample. Run-to-run variance is somewhat
 764 larger for these configurations, while using $d \geq 5$ yields stable ARE
 765 performance regardless of k . Absolute error increases with more
 766 rows for any fixed k , as each per-row estimator has fewer buckets,
 767 inducing more collisions and updates per KLL, in turn leading to
 768 more compactions and more items evicted from KLLs.

769 Based on these results, we select $k = 10$ and $d = 4$ for subsequent
 770 experiments, to balance throughput and accuracy. From the analysis
 771 (Theorem 7), the choice of k does not impact the worst-case error
 772 bound, hence we select k based on the empirical results observed
 773 here. We observe that smaller k has significantly better accuracy
 774 with only a minor impact on throughput. Although a smaller k
 775 entails more frequent KLL compaction, the larger w permitted in
 776 the same M yields overall better accuracy (many small KLLs with

³Open-source, available at <https://github.com/vinhqng05/ReSketch>, [26]

fewer collisions is more accurate than fewer large ones) in both ARE and AAE. Similarly, selecting a low depth d permits a larger w in the same M , reducing collisions per row hence yielding better per-row estimators to take the median over.

6.2 Benchmarks

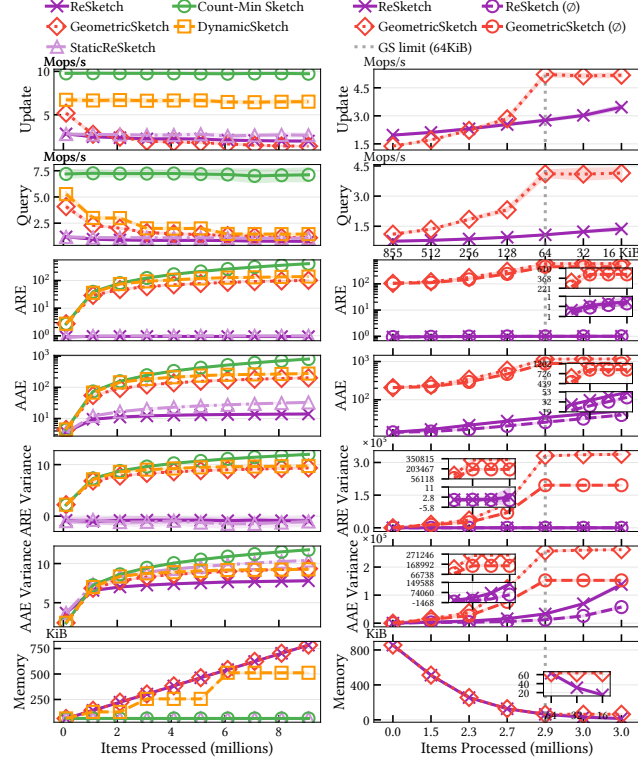


Figure 6: Comparison of performance subject to resizing operations compared to baselines (partially) supporting them; expand on the left and shrink on the right.

6.2.1 Resize. We evaluate the performance of RESENCH when resizing, in terms of throughput and accuracy. We compare with the resizable baselines as well as a static, non-resized CMS and RESENCH instance to see potential performance or accuracy changes due to resizing, while highlighting the benefit of resizability compared to using a static sketch configuration.

Method. The benchmark proceeds in two phases. First, all sketches are initialized at $M_0 = 64$ KiB (as in the sensitivity analysis), and begin processing updates while recording update throughput. After every 100 k updates, we measure ARE, AAE, within-run variance, and query throughput. Then, the memory budget for each sketch is expanded by $M_\Delta = 8$ KiB, and the process continues until 10 M items have been processed and the sketches have grown to $M_1 = 864$ KiB. Note that DCMS only expands once the budget has doubled, due to the coarse-grain expansion scheme used. The second phase, using copies of the previously populated sketches, proceeds with a series of shrink operations to a final size of $M_2 = 16$ KiB. Accuracy is again recorded after each shrink. One copy of each sketch is kept pristine (denoted \emptyset), while the other receives additional updates in

between shrink operations to determine the impact of shrinking both in isolation and in conjunction with data manipulation.

Results. Figure 6 shows results in all metrics for the expand and shrink phases on the left and right, respectively. Update throughput of RESENCH decreases as the sketch size outgrows L2 cache, but stays close to the static RESENCH, while GS decays more as the sketch expands further. CMS and DCMS utilize less complex hashing schemes and are therefore able to sustain higher update throughput, while query throughput for DCMS degrades significantly as the chain of internal CMS instances grows. In comparison to baseline approaches, RESENCH achieves orders of magnitude improved accuracy. AAE and its variance reveal the benefit of expansion on accuracy when processing the same input, permitting the sketch to store more heavy items in the buckets, shown by the increasing gap between RESENCH and the static variant.

In the shrink phase, throughput of RESENCH increases as the sketch shrinks. GS cannot shrink below its initial size M_0 , and hence stagnates there while RESENCH continues to shrink down to M_2 (bottommost figure). RESENCH again exhibits lower estimation errors, also in presence of continued update operations, while error increases significantly for GS if updates are performed.

6.2.2 EnhancedMerge & Partition. We proceed to evaluate the performance of RESENCH EnhancedMerge and Partition operations. The aim is to compare the impact of these operations on estimation error. No baseline supports partitioning, hence these operations are benchmarked in isolation, while parameters are selected to align with the results of the sensitivity analysis.

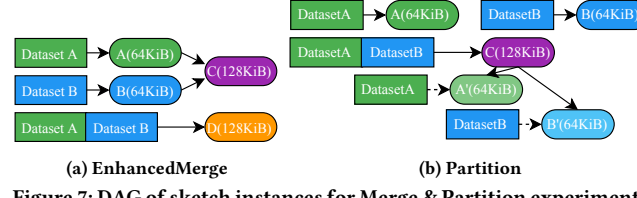


Figure 7: DAG of sketch instances for Merge & Partition experiments.

Method. To this end, Figure 7 shows two DAGs of input datasets, sketch instances, and the structure-defining operations that link them. For both experiments, again a base memory budget of $M = 64$ KiB is assigned. For the EnhancedMerge experiment, the input dataset is partitioned into Dataset A (DA) and Dataset B (DB), and processed to yield sketches A and B, respectively. A and B are then merged to produce sketch C with a size of 128 KiB. The accuracy of queries C is then compared that of queries on a 128 KiB baseline sketch D, which receives the full input dataset.

For the Partition experiment, the input dataset is summarized in a sketch C (64 KiB) which is then partitioned into sketches A' and B', of half the size each, acting as if they had processed only their respective partition of the dataset. The accuracy of these sketches is compared to ‘ground truth’ sketches A and B, which each have processed the corresponding partition of the input data.

Results. The relative and absolute error of every unique item in the input dataset (ordered by rank) are shown in Figure 8. Accuracy of merged sketch C, produced from merging two partition sketches A and B, is very similar to that of sketch D which has processed the complete input itself, as well as of A and B (shown in Table 3 as ARE and AAE along with run-to-run variances), as expected from

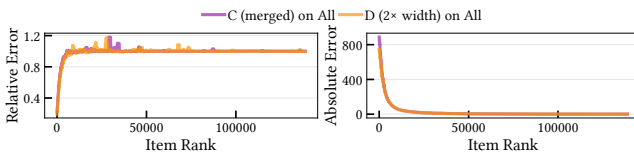


Figure 8: Accuracy after EnhancedMerge.

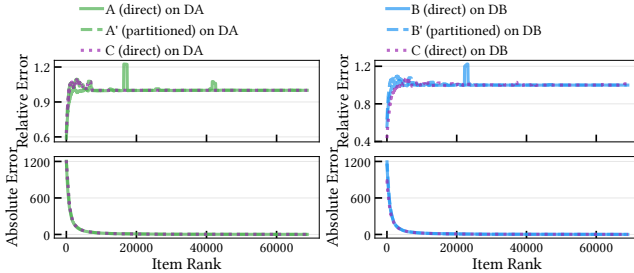


Figure 9: Accuracy after Partition.

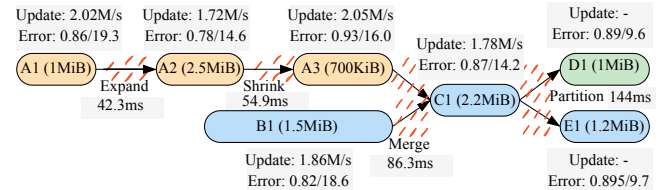


Figure 10: Application execution modelled as DAG (Figure 4). Gray boxes contain performance results; nodes (sketch instances) are annotated with achieved update throughput and accuracy (ARE/AAE), edges (structure-defining operations) with latency.

Results. The results are shown in Figure 10. The asymptotic complexities are reflected in the small latencies for structure-defining operations, which are expected to be invoked much less frequently than data manipulation; expand and shrink and merge are all similar, scaling depending on their input size, while the complexity of Partition and the size of its inputs determine its 144 ms latency.

Key Takeaways From Evaluation

Summary: (1) Sensitivity analysis reveals the balancing trade-off between memory, accuracy, and performance, showing how to allocate that memory between M , w , and k . (2) Importantly, the analysis shows the benefit of using multiple smaller KLL instances per row, aligning with and extending earlier results [18, 20, 27, 32] about partitioning leading to better memory-accuracy ratios. (3) Resize, EnhancedMerge, and Partition are a powerful set of operations for supporting elasticity; they maintain their theoretical accuracy and performance as per the lemmas in § 5 also in realistic benchmarks. (4) A realistic use-case for ReSKETCH is evaluated to demonstrate its suitability for real-world applications. These results show the suitability of ReSKETCH for long-lived data analytics processes with dynamic memory availability, due to its ability to be resized, partitioned, and merged dynamically during execution. The sketch maintains its throughput performance and accuracy throughout these operations, while growing into available memory to improve estimation accuracy, or shrinking to free up memory for other work, continuing to process items while maintaining orders of magnitude better accuracy than prior methods. ReSKETCH natively captures the dynamic nature of distributed monitoring systems through corresponding structure-defining operations, addressing the gap left by limitations in existing approaches which lack the necessary generalized flexibility.

7 CONCLUSIONS

ReSKETCH is a novel sketch algorithmic design that delivers three critical properties – *resizability*, *enhanced mergeability*, and *partitionability*. Beyond that, this work also lays the foundation for analyzing approximation error in dynamic distributed sketches through the *instance provenance DAG*, a formal framework that enables to reason about and bound the approximation error of sketch instances produced by arbitrary sequences of operations, which is really important to ensure that the resulting sketches maintain rigorous guarantees. Empirically, ReSKETCH demonstrates high accuracy and competitive throughput on evaluation, validating its practicality. By offering a blueprint for transforming rigid matrix-based sketches into (enhanced) mergeable, partitionable, and resizable structures, we believe ReSKETCH paves the way for a new generation of adaptive approximate query processing systems capable of seamless elastic scaling and rebalancing.

849 Lemma 13. Similarly, for Partition, Figure 9 shows the accuracy
 850 for the two dataset partitions DA and DB achieved by partitioned
 851 sketches A' and B' compared to the respective baseline sketches A
 852 and B, again exhibiting very similar accuracy. Table 4 shows the
 853 estimation accuracy of each sketch instance. We also compare with
 854 the larger ancestor sketch C, and find that the partition operation
 855 has succeeded in maintaining the accuracy that could be achieved
 856 by querying C for the respective partition's items (cf. Lemma 14).

Table 3: EnhancedMerge accuracy.

Sketch	ARE	AAE
A	0.9919 ± 0.0017	27.95 ± 0.39
B	0.9914 ± 0.0034	25.96 ± 0.35
C	0.9927 ± 0.0021	27.09 ± 0.26
D	0.9898 ± 0.0019	25.69 ± 0.27

Table 4: Partition accuracy.

Sketch	ARE	AAE
A'	0.9994 ± 0.0017	37.05 ± 0.87
B'	0.9977 ± 0.0024	30.89 ± 0.70
A	0.9970 ± 0.0026	34.73 ± 1.03
B	0.9967 ± 0.0017	34.33 ± 0.91
C	0.9957 ± 0.0014	33.00 ± 0.44

6.3 Application Example

Finally, we evaluate the performance of ReSKETCH for supporting a realistic end-to-end application (Figure 1) requiring all types of structural operations. We consider a representative execution of this system, shown in Figure 4, which prior work could not support.

Method. Each processing period (node) processes 2 M items from the CAIDA dataset (except D1 and E1 which process no more updates). Update throughput and query accuracy in terms of ARE and AAE is recorded for each processing period, and the latency of each structure-defining operation is measured.

Execution begins with one node (yellow in the DAG) summarizing an input stream to A1, and as more data arrives and ample memory is available, the sketch is expanded to A2 to improve accuracy as the process continues. After some time, a second node (blue) joins the system and begins processing a separate data stream in sketch B1. Meanwhile, the first node has to reallocate memory to a higher priority task, and the sketch relinquishes a large fraction of its memory. Eventually, node 1 departs from the system, so all processing is moved to the second node, and the two active sketch instances are merged to form C1. Finally, a new node (green) arrives, and the large C1 sketch is partitioned into D1 and E1 to load balance over both available nodes according to their capacities.

REFERENCES

- [1] Swarup Acharya, Phillip B. Gibbons, Viswanath Poosala, and Sridhar Rama-swamy. 1999. Join synopses for approximate query answering. In *Proceedings of the 1999 ACM SIGMOD international conference on Management of data (SIGMOD '99)*. Association for Computing Machinery, New York, NY, USA, 275–286. <https://doi.org/10.1145/304182.304207>
- [2] Pankaj K. Agarwal, Graham Cormode, Zengfeng Huang, Jeff Phillips, Zhewei Wei, and Ke Yi. 2012. Mergeable summaries. In *Proceedings of the 31st ACM SIGMOD-SIGACT-SIGAI symposium on Principles of Database Systems (PODS '12)*. Association for Computing Machinery, New York, NY, USA, 23–34. <https://doi.org/10.1145/2213556.2213562>
- [3] Noga Alon, Phillip B. Gibbons, Yossi Matias, and Mario Szegedy. 1999. Tracking join and self-join sizes in limited storage. In *Proceedings of the eighteenth ACM SIGMOD-SIGACT-SIGART symposium on Principles of database systems (PODS '99)*. Association for Computing Machinery, New York, NY, USA, 10–20. <https://doi.org/10.1145/303976.303978>
- [4] Dvir Biton, Roy Friedman, and Rana Shahout. 2025. Geometric Sketch: The Inflatable-Shrinkable Sketch. In *Advanced Information Networking and Applications*, Leonard Barolli (Ed.). Springer Nature Switzerland, Cham, 270–281. https://doi.org/10.1007/978-3-031-87766-7_24
- [5] Burton H. Bloom. 1970. Space/time trade-offs in hash coding with allowable errors. *Commun. ACM* 13, 7 (July 1970), 422–426. <https://doi.org/10.1145/362686.362692>
- [6] CAIDA. 2018. The CAIDA UCSD Anonymized Internet Traces - 2018-03-15. https://catalog.caida.org/dataset/passive_2018_pcaps
- [7] Moses Charikar, Kevin Chen, and Martin Farach-Colton. 2004. Finding frequent items in data streams. *Theoretical Computer Science* 312, 1 (Jan. 2004), 3–15. [https://doi.org/10.1016/S0304-3975\(03\)00400-6](https://doi.org/10.1016/S0304-3975(03)00400-6)
- [8] Yann Collet. 2026. xxHash. <https://github.com/Cyan4973/xxHash>
- [9] Graham Cormode and Minos Garofalakis. 2005. Sketching streams through the net: distributed approximate query tracking. In *Proceedings of the 31st international conference on Very large data bases (VLDB '05)*. VLDB Endowment, Trondheim, Norway, 13–24. <https://dl.acm.org/doi/abs/10.5555/1083592.1083598>
- [10] Graham Cormode and Marios Hadjieleftheriou. 2008. Finding frequent items in data streams. *Proc. VLDB Endow.* 1, 2 (Aug. 2008), 1530–1541. <https://doi.org/10.14778/1454159.1454225>
- [11] Graham Cormode and S. Muthukrishnan. 2005. An improved data stream summary: the count-min sketch and its applications. *Journal of Algorithms* 55, 1 (April 2005), 58–75. <https://doi.org/10.1016/j.jalgor.2003.12.001>
- [12] Graham Cormode and S. Muthukrishnan. 2005. Summarizing and Mining Skewed Data Streams. In *Proceedings of the 2005 SIAM International Conference on Data Mining*. Society for Industrial and Applied Mathematics, Newport Beach, CA, USA, 44–55. <https://doi.org/10.1137/1.9781619727575>
- [13] Ted Dunning. 2021. The t-digest: Efficient estimates of distributions. *Software Impacts* 7 (Feb. 2021), 100049. <https://doi.org/10.1016/j.simpa.2020.100049>
- [14] Minos Garofalakis, Johannes Gehrke, and Rajeev Rastogi (Eds.). 2016. *Data Stream Management: Processing High-Speed Data Streams*. Springer, Berlin, Heidelberg. <https://doi.org/10.1007/978-3-540-28608-0>
- [15] Anna C. Gilbert, Yannis Kotidis, S. Muthukrishnan, and Martin Strauss. 2001. Surfing Wavelets on Streams: One-Pass Summaries for Approximate Aggregate Queries. In *Proceedings of the 27th International Conference on Very Large Data Bases (VLDB '01)*. Morgan Kaufmann Publishers Inc., San Francisco, CA, USA, 79–88.
- [16] Liyuan Gu, Ye Tian, Wei Chen, Zhongxiang Wei, Cenman Wang, and Xinxing Zhang. 2024. Per-Flow Network Measurement With Distributed Sketch. *IEEE/ACM Transactions on Networking* 32, 1 (Feb. 2024), 411–426. <https://doi.org/10.1109/TNET.2023.3286879>
- [17] Dor Harris, Arik Rinberg, and Ori Rottenstreich. 2023. Compressing Distributed Network Sketches With Traffic-Aware Summaries. *IEEE Transactions on Network and Service Management* 20, 2 (June 2023), 1962–1975. <https://doi.org/10.1109/TNSM.2022.3172299>
- [18] Martin Hilgendorf and Marina Papatriantafilou. 2025. LMQ-Sketch: Lagom Multi-Query Sketch for High-Rate Online Analytics. In *39th International Symposium on Distributed Computing (DISC 2025) (Leibniz International Proceedings in Informatics (LIPIcs))*, Dariusz R. Kowalski (Ed.), Vol. 356. Schloss Dagstuhl – Leibniz-Zentrum für Informatik, Dagstuhl, Germany, 36:1–36:24. <https://doi.org/10.4230/LIPIcs.DISC.2025.36>
- [19] Nikita Ivkin, Edo Liberty, Kevin Lang, Zohar Karnin, and Vladimir Braverman. 2019. Streaming Quantiles Algorithms with Small Space and Update Time. [https://doi.org/10.48550/arXiv.1907.00236 \[cs\]](https://doi.org/10.48550/arXiv.1907.00236)
- [20] Victor Jarlow, Charalampos Stylianopoulos, and Marina Papatriantafilou. 2025. QPOPSS: Query and Parallelism Optimized Space-Saving for finding frequent stream elements. *J. Parallel and Distrib. Comput.* 204 (Oct. 2025), 105134. <https://doi.org/10.1016/j.jpdc.2025.105134>
- [21] David Karger, Eric Lehman, Tom Leighton, Rina Panigrahy, Matthew Levine, and Daniel Lewin. 1997. Consistent hashing and random trees: distributed caching protocols for relieving hot spots on the World Wide Web. In *Proceedings of the twenty-ninth annual ACM symposium on Theory of computing - STOC '97*. ACM Press, El Paso, Texas, United States, 654–663. <https://doi.org/10.1145/258533.258660>
- [22] Zohar Karnin, Kevin Lang, and Edo Liberty. 2016. Optimal Quantile Approximation in Streams. In *2016 IEEE 57th Annual Symposium on Foundations of Computer Science (FOCS)*. IEEE, New Brunswick, NJ, USA, 71–78. <https://doi.org/10.1109/FOCS.2016.17>
- [23] Ahmed Metwally, Divyakant Agrawal, and Amr El Abbadi. 2006. An integrated efficient solution for computing frequent and top-k elements in data streams. *ACM Trans. Database Syst.* 31, 3 (Sept. 2006), 1095–1133. <https://doi.org/10.1145/1166074.1166084>
- [24] J. Misra and David Gries. 1982. Finding repeated elements. *Science of Computer Programming* 2, 2 (Nov. 1982), 143–152. [https://doi.org/10.1016/0167-6423\(82\)90012-0](https://doi.org/10.1016/0167-6423(82)90012-0)
- [25] Michael Mitzenmacher and Eli Upfal. 2012. *Probability and computing: randomized algorithms and probabilistic analysis*. Cambridge University Press, Cambridge.
- [26] Vinh Quang Ngo and Martin Hilgendorf. 2025. ReSketch: A Mergeable, Redistributable, and Resizable Sketch. <https://github.com/vinhqng05/ReSketch>
- [27] Vinh Quang Ngo and Marina Papatriantafilou. 2025. Cuckoo Heavy Keeper and the Balancing Act of Maintaining Heavy Hitters in Stream Processing. *Proceedings of the VLDB Endowment* 18, 9 (May 2025), 3149–3161. <https://doi.org/10.14778/3746405.3746434>
- [28] Odysseas Papapetrou, Minos Garofalakis, and Antonios Deligiannakis. 2012. Sketch-based querying of distributed sliding-window data streams. *Proc. VLDB Endow.* 5, 10 (June 2012), 992–1003. <https://doi.org/10.14778/2336664.2336672>
- [29] Wieger R. Punter, Odysseas Papapetrou, and Minos Garofalakis. 2023. OmniSketch: Efficient Multi-Dimensional High-Velocity Stream Analytics with Arbitrary Predicates. *Proc. VLDB Endow.* 17, 3 (Nov. 2023), 319–331. <https://doi.org/10.14778/3632093.3632098>
- [30] Nicolò Rivetti, Leonardo Querzoni, Emmanuelle Anceaume, Yann Busnel, and Bruno Sericola. 2015. Efficient key grouping for near-optimal load balancing in stream processing systems. In *Proceedings of the 9th ACM International Conference on Distributed Event-Based Systems*. ACM, Oslo Norway, 80–91. <https://doi.org/10.1145/2675743.2771827>
- [31] Qilong Shi, Yuchen Xu, Jiahua Qi, Wenjun Li, Tong Yang, Yang Xu, and Yi Wang. 2023. Cuckoo Counter: Adaptive Structure of Counters for Accurate Frequency and Top-k Estimation. *IEEE/ACM Transactions on Networking* 31, 4 (Aug. 2023), 1854–1869. <https://doi.org/10.1109/TNET.2022.3232098>
- [32] Charalampos Stylianopoulos, Ivan Walulya, Magnus Almgren, Olaf Landsiedel, and Marina Papatriantafilou. 2020. Delegation sketch: a parallel design with support for fast and accurate concurrent operations. In *Proceedings of the Fifteenth European Conference on Computer Systems (EuroSys '20)*. Association for Computing Machinery, New York, NY, USA, 1–16. <https://doi.org/10.1145/3342195.3387542>
- [33] Mikkel Thorup. 2020. High Speed Hashing for Integers and Strings. [https://doi.org/10.48550/arXiv.1504.06804 \[cs\]](https://doi.org/10.48550/arXiv.1504.06804) version: 9.
- [34] xxHash Contributors. 2024. Performance comparison - Benchmarks concentrating on small data. <https://github.com/Cyan4973/xxHash/wiki/Performance-comparison/c624714b9a0d455eb474c7ae3f92864451d7b4be#benchmarks-concentrating-on-small-data->
- [35] Tong Yang, Junzhi Gong, Haowei Zhang, Lei Zou, Lei Shi, and Xiaoming Li. 2018. HeavyGuardian: Separate and Guard Hot Items in Data Streams. In *Proceedings of the 24th ACM SIGKDD International Conference on Knowledge Discovery & Data Mining (KDD '18)*. Association for Computing Machinery, New York, NY, USA, 2584–2593. <https://doi.org/10.1145/3219819.3219978>
- [36] Tong Yang, Jie Jiang, Peng Liu, Qun Huang, Junzhi Gong, Yang Zhou, Rui Miao, Xiaoming Li, and Steve Uhlig. 2018. Elastic sketch: adaptive and fast network-wide measurements. In *Proceedings of the 2018 Conference of the ACM Special Interest Group on Data Communication (SIGCOMM '18)*. Association for Computing Machinery, New York, NY, USA, 561–575. <https://doi.org/10.1145/3230543.3230544>
- [37] Tong Yang, Haowei Zhang, Jinyang Li, Junzhi Gong, Steve Uhlig, Shigang Chen, and Xiaoming Li. 2019. HeavyKeeper: An Accurate Algorithm for Finding Top-k Elephant Flows. *IEEE/ACM Transactions on Networking* 27, 5 (Oct. 2019), 1845–1858. <https://doi.org/10.1109/TNET.2019.2933868>
- [38] Xiaobo Zhu, Guangjun Wu, Hong Zhang, Shupeng Wang, and Bingnan Ma. 2018. Dynamic Count-Min Sketch for Analytical Queries Over Continuous Data Streams. In *2018 IEEE 25th International Conference on High Performance Computing (HiPC)*. IEEE Computer Society, Bengaluru, India, 225–234. <https://doi.org/10.1109/HiPC.2018.00033>